Natural silicate-TiO_2 hybrids for photocatalytic oxidation of formaldehyde in gas phase

R. Portela[a], I. Jansson[b], S. Suárez[b], M. Villarroel[c], B. Sánchez[b] and P. Ávila**

a) Institute for Catalysis and Petrochemistry, CSIC, Madrid 28049, Spain

b) FOTOIR Group, Renewable Energy Division CIEMAT, Madrid 28040, Spain

c) Santiago de Chile University, Faculty of Chemistry and Biology, Santiago, P.C. 9170022, Chile

Corresponding authors: silvia.suarez@ciemat.es; pavila@icp.csic.es*

Graphical abstract

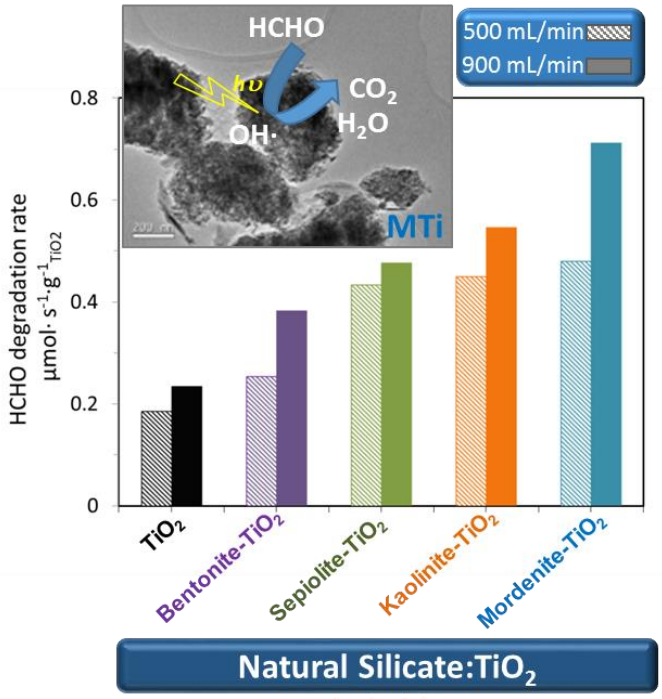

Highlights:

- Natural silicates allow the extrusion of monoliths containing photoactive titania.
- The hybrid materials improve HCHO photooxidation rate compared to bare TiO_2.
- The exposed fraction of TiO_2 on the structure is a key factor for HCHO elimination.
- HCHO photocatalytic removal is promoted on high aluminum content silicate-TiO_2.

Abstract

Structured hybrid materials based on the combination adsorbent-photocatalyst with optimal mechanical resistance and reduced cost, are prepared by extrusion using four different natural silicates with similar mesoporous distribution: sepiolite (S), bentonite (B), mordenite (M) and kaolinite (K). The effect of the textural, morphological and structural properties of plate shaped composites calcined at different temperatures on the adsorption and photocatalytic degradation of formaldehyde in gas phase is analysed. Silicates allows TiO_2 extrusion into flat plates with a content of 50 wt. % of titania. All shaped materials present adequate mechanical resistance to be scaled-up for use in continuous-flow gas-phase catalytic reactors. Thermal treatment at 500 ºC ensures an optimum combination of mechanical, textural and HCHO adsorption properties. The silicates cover part of the TiO_2 particles thus reducing the fraction of TiO_2 actually exposed on the surface of the composites, essential to carried out the photocatalytic process, but they also allow controlling TiO_2 dispersion and the amount of HCHO adsorbed. The HCHO degradation rate is enhanced with all the silicate-TiO_2 composites with respect to that of the benchmark TiO_2. The incorporation of titania into the silicate matrix favors the gas phase removal of HCHO in the following sequence: MTi > KTi > STi > BTi > TiO_2. The exposed fraction of titania particles and the size of the TiO_2-anatase crystalline domains determine the efficiency of the hybrid material, which is optimized in high-aluminium kaolinite and mordenite based hybrids.

Keywords

Photocatalysis; TiO_2; natural silicate; adsorbent-photocatalyst hybrids; formaldehyde; VOC.

1. Introduction

Heterogeneous photocatalysis is a feasible alternative to reduce the air pollution impact [1], competing in many applications with conventional air treatment technologies such as adsorption, filtering, combustion or thermal catalysis, particularly for low-flow and low-concentration emissions [2]. Laboratory results have demonstrated that photocatalysis is suitable for the abatement of most pollutants [3], and thus the implementation of photocatalytic systems for air treatment is nowadays attractive for the industry [4]. Formaldehyde (HCHO) is one of the major sources of indoor air pollution, contributing to the "sick building syndrome" [5, 6] and an intermediate of the photocatalytic oxidation reaction of other volatile organic compounds (VOCs) [7]. Irritation of eyes, throat and the respiratory track, sneezing, and coughing are some of its effects on the human health. Adhesives, resins and glues used in the manufacture of wooden products (furniture and plywood) and foam insulators can be cited amongst the main anthropogenic formaldehyde sources. Therefore, the study of its photocatalytic degradation has captured the interest of the scientific community.

One of the main obstacles for the widespread implementation of industrial application of photocatalytic technologies is its low photocatalytic efficiency. To overcome this limitation, efforts should be focused on the optimization of the photoreactor design by improving mass and photon transfer limitations, and the improvement of the photocatalytic configuration [8]. In the field of air pollution control the use of ultrafine photocatalytic powders, with large specific surface area, presents practical drawbacks such as the need for expensive and energy consuming fluidization and recovery processes. A way of intensification of the photocatalytic process is to immobilize the semiconductor on a high surface area substrate without significant loss of photocatalytic activity. This conformation allows to improve the dispersion of the active phase, the photon transfer process to the active sites and to reduce the amount of the photoactive phase [9]. In this line, adsorbent–photocatalyst hybrids (APHs) are promising bi-functional immobilized photocatalysts for environmental applications. The synergy between adsorption and photoactivity may lead to composites with improved performance, including superior conversion and selectivity to the desired reaction products [10]. The adsorbent acts as a support, immobilizing and dispersing the active phase, thereby increasing the surface area of the final solid and facilitating the shaping of the material. Additionally, it may also induce modifications that may promote physicochemical processes, for example in the

acid–base character or UV light absorption properties or the crystallinity of the semiconductor. Aiming at the advantages of structured solid catalysts, in the early nineties the first studies on TiO_2-coated ceramic monoliths as photocatalysts appeared [11, 12], and a couple of years later the first monoliths with incorporated TiO_2 were investigated [13-15]. Since the early works of Yoneyama *et al.* in the nineties on the photocatalytic properties of adsorbent-TiO_2 composites in water and air [16] many articles have been published in the literature describing the properties of different APHs materials. On the semiconductor side, and for environmental and commercial applications, the properties of TiO_2 make of it still the most reasonable option as photocatalyst [10]. On the side of the adsorbent support, many materials have been proposed. For instance, Bouazza *et al.* compared the performance of pelletized TiO_2 and the mixtures with activated carbon, zeolites, MCM-41, a metal-organic framework, SiO_2, Al_2O_3, glass wool, and quartz wool for propene oxidation [17]. Mo et al. compared the properties of TiO_2 combined with zeolites, silica and alumina for the degradation of toluene in air [18]. It is generally assumed that the photocatalytic reaction rate constant for different pollutants correlates with their adsorption capacity [19]. On the other hand, selecting low-cost raw materials and green synthesis routes is required to make of APHs commercially and environmentally viable solutions. Taking these features into account, carbonaceous [20] and siliceous [21, 22] materials with different structures and morphologies are generally the most attractive supports for adsorbent–photocatalytic hybrids. Among the silicates, several natural layered clays are of prime interest [23], because they are chemically inert, resistant and available in large quantities. For instance, AHPs based on kaolinite give promising results for photodisinfection [24] and photodegradation of organic compounds [25], Ti-pillared montmorillonite showed better photocatalytic performance compared to benchmark TiO_2 for degradation of several pollutants both in water and air phases [26, 27] and TiO_2−sepiolite nanocomposites present a potential application as photocatalyst [28]. Additionally, the silicate may present large surface area and porosity, high concentration of hydroxyl groups, and suitable rheological properties for extrusion of monolithic conformations [29, 30]. Natural sepiolite-TiO_2 APHs conformed as plate-shaped monoliths showed excellent photocatalytic properties for removal of volatile organic compounds, such as trichloroethylene [31], or inorganic pollutants, such as hydrogen sulfide [32], under artificial or solar radiation [33, 34]. Compared to the final impregnation of the photocatalyst onto the extruded sepiolite structure, its incorporation into the bulk of the dough by mixing before extrusion, has demonstrated to promote

mineralization, avoiding the formation of undesirable reaction products [35]. Additionally, this preparation method meets simplicity and economy criteria required in industrial processes, which are not fulfilled by traditional, yet significantly more complex methods such as pillarization, sol-gel, etc. On the other hand, although internal surface accessibility is favored in these hybrid solids if the semiconducting particles are incorporated by pillaring [29] or delaminating [30] the clays, the aforementioned properties are also affected by these processes, [36, 37]. In this work, four natural silicates with similar porous distribution and different chemical structure and composition are studied as components of TiO_2-based adsorbent-photocatalyst hybrids. Two of them are based on 2:1 phyllosilicates with magnesium: layered bentonite (with ideal formula $(Na,Ca)_{0.33}(Al,Mg)_2(Si_4O_{10})$) and sepiolite (a fibrous tectosiliate with general formula $Mg_4Si_6O_{15}(OH)_2 \cdot 6H_2O$), and the other two on aluminium silicates: kaolinite ($Al_2Si_2O_5(OH)_4$) a layered 1:1 silicate, and mordenite ($(Ca,Na_2,K_2)Al_2Si_{10}O_{24} \cdot 7H_2O$) as tectosilicate with zeolitic structure. The influence of the physicochemical properties of these binary systems in their adsorption ability and in the photocatalytic degradation of formaldehyde in gas phase is analysed.

2. Experimental Section

2.1 Adsorbent–photocatalyst hybrids preparation

Four natural silicates were used to prepare TiO_2-based 50 wt.% adsorbent-photocatalyst hybrids. TiO_2 and the natural silicate were mixed and kneaded with the necessary amount of water to obtain an extrudable paste. The amount of water depends on the ability of each material to adsorb water and to incorporate it into the structure, ranging between 37 wt.% and 48 wt.%. The extrusion machine was operated at atmospheric pressure at 10 r.p.m. Plates of 80 x 24 x 3 mm were extruded, dried at room temperature, and then heat treated in air atmosphere at 300, 500 and 800 °C for 4 h. The samples are referred to as YTi, where Ti stands for anatase TiO_2 (G5, Millenium/Cristal) with high-surface area (370 m^2 g^{-1}, $SO_3^{:}$ ~ 0.6 wt%,), and Y can be: B, standing for smectite-type bentonite (Atox, 95% purity, Tolsa); K, for a kaolinitic clay (Hymod Excelsior, ECC/Imerys); M, for high-purity silica-rich mordenite-type zeolite (Benesa) [38], or S, for sepiolite (Pansil 100, 60% purity, Tolsa) [39]. Finally, the numeric suffix indicates the temperature of the heat treatment.

2.2 Physicochemical characterization

N_2 adsorption/desorption isotherms, obtained at −196 °C in an ASAP 2420 apparatus (Micromeritics), and *mercury intrusion porosimetry* (MIP), performed in an AutoPore IV 9510 mercury intrusion/extrusion porosimeter (Micromeritics), were employed for the textural characterization of the composites. Specific surface area data were calculated by application of the BET equation to the adsorption branch of nitrogen isotherms. The external surface area was obtained from MIP. Pore volume and pore size distribution curves combine MIP (in the meso- and macro-pore range) and N_2 isotherms (micro- and meso-pore range) data. Pore size was calculated using the Washburn equation for cylindrical pores. The chemical composition of the hybrid composites was determined by *inductively coupled plasma-optical emission spectroscopy* (ICP-OES) of acid solutions of the ground materials in a Perkin–Elmer Optima 3300DV apparatus. *TGA-DTA* analysis were performed using a STA 6000 (Perkin Elmer) , in an air flow of 50 mL min^{-1} with a heating rate of 10 ºC min^{-1} between 25ºC-900ºC with samples of ca. 25 mg. Morphological and semi quantitative chemical analyses of the external surface were performed on small pieces of the as-prepared solids by *scanning electron microscopy* (SEM) and energy dispersive X-ray spectroscopy (EDX) in a JEOL JSM 6400 30 kV scanning microscope with a tungsten filament thermionic cathode electron beam, a INCA Oxford instruments X-Man^N detector, and a standard window, equipped with an EXD Link eXL analyser with a 25 keV electron beam and a take-off angle of 45º. The samples were coated with a conductive layer of graphite to minimize charging effects. The *transmission electron microscopy* studies of the samples crushed into fine powders were carried out in a JEM JEOL 2100HT, operated at 200 kV. The images were recorded with a CCD camera ORIUS SC1000 (Model 832, GATAN).

A basic characterization of the crystalline structure was made from the *X-ray diffraction* (XRD) patterns obtained with a PANalytical X'Pert Pro diffractometer, using Ni-filtered Cu K_α radiation with λ = 1.5406 nm; the mean anatase-TiO_2 crystallite sizes were estimated using the Scherrer's equation. *UV–vis diffuse reflectance spectroscopy* measurements were performed on a Shimadzu UV2100 apparatus using $BaSO_4$ as a reference. The *mechanical resistance* of the samples was evaluated by measuring the crushing strength with a Chatillon dynamometer (broach diameter = 1 mm). The rupture pressure (σ) was calculated as the ratio between the maximum force applied before breaking (F) and the area of the broach (S = 7.8 x 10^{-7} m^2). The measurements were

repeated at least ten times on various samples to secure statistically significant values. The structural resistance of the plates to water was tested immersing the samples in water for 15 min. Zeta potential measurements were performed by electrophoretic migration with a Zeta Meter 3.0 and a Zetasizer Nano ZS90 with a MPT-2 autotitrator, using 30 mg of sample suspended in 300 mL of a 10^{-3} M KCl solution. The pH was adjusted with HCl or NaOH solutions. Each curve was recorded at least three times to ensure reproducibility.

2.3 Evaluation of the photocatalytic activity

In a first stage, experiments were performed with small pieces of ceramic plates. Nevertheless, the long periods required for saturation and stabilization of the reaction conditions before and after irradiation (more than 24 h), due to the large adsorption ability of the hybrids and the high proportion of non-irradiated material, led to a change in the experimental procedure. Then, the photocatalytic vs. adsorption effect was maximized using only 0.03 g of powder material spread on a large surface to carry out the photocatalytic tests. The experiments conducted with either crushed or non–crushed materials showed the same trend. The APH based plates were first crushed into powder, and 0.03 g of each sample was suspended in isopropanol to disperse it on a glass surface of 17.3 cm^2. Subsequently, the samples were heated at 100 ˚C to remove the solvent. Moreover, they were then irradiated under UV-A during 12 h in an air flow of 200 mL min^{-1} in order to eliminate any possible residual organic compound. The supported powdered sample was introduced in a flat reactor previously described [31], irradiated by two UVA 8W lamps (Philips). A continuous N_2 stream containing 10.5% O_2 and 15 ppm of formaldehyde (a 50 vol.% mix of compressed air and 30 ppm HCHO/N_2 gas supplied from a calibrated cylinder, Air Liquide) was fed to the reactor. The gas composition was analysed on-line in a FTIR spectrometer (Nicolet, Thermo) equipped with a gas cell; the integrated area of the IR absorption bands of HCHO (1,842-1,623 cm^{-1}) and CO_2 (2,400-2,260 cm^{-1}) was used for the quantitative analysis. The adsorption capacity of the materials was determined at a flow rate of 700 mL min^{-1} using a UV cut off filter, to avoid any photocatalytic activity maintaining the same temperature as in the photocatalytic tests (T = 35 ºC). Once the dynamic adsorption equilibrium was reached, the UV-filter was removed and the photocatalytic activity was evaluated at flow rates between 100-900 mL min^{-1} (tr = 3.9-0.6 s). The irradiance measured on the photocatalyst surface was 11 mW cm^{-2}.

3. Results and Discussion

Pure TiO_2 cannot be shaped because the dough prepared from the mixture of titania and water does not have suitable rheological properties. However, all the natural silicates under study have adequate rheological properties as binders and allowed the extrusion of high-titania-content (50 wt.%) ceramic plates that were dried and calcined at 300, 500 and 800 ºC without damage. These solids have been thoroughly analyzed to evaluate their potential as photocatalysts.

3.1 Characterization results

3.1.1 Mechanical resistance of ceramic plates

In **Figure 1**, the mechanical strength values of the 50 wt.% silicate-TiO_2 ceramic flat plates heat treated at different temperatures are shown. According to the crushing strength results, all the hybrids present good mechanical resistance, one of the main properties required for their industrial application. Although higher temperature treatments lead to more resistant ceramic plates, the crushing strength is higher than 100 kg cm^{-2} for all compositions (except for KTi-300) at every temperature studied. This property depends on several factors, such as the nature of the raw materials, the applied extrusion pressure, or the geometry of the extrudate, amongst others. Moreover, the values obtained depend on the axis on which the force is applied (axial or radial compression) [40]. Normal axial compression values for pellets range between 10-100 kg cm^{-2} [41], and according to our previous results with ceramic materials, values above 50 kg cm^{-2} ensure a proper handling to be employed in scaled-up continuous-flow gas-phase catalytic reactors [33, 34]. Sepiolite and bentonite give the most resistant materials, with crushing strength values around 600 kg cm^{-2}. Moreover, all samples treated at 500 and 800 ºC, with exception of KTi-500, withstand the immersion in water, and thus tolerate their use in condensing environments or further wet impregnation processes to add active phases on the materials surface.

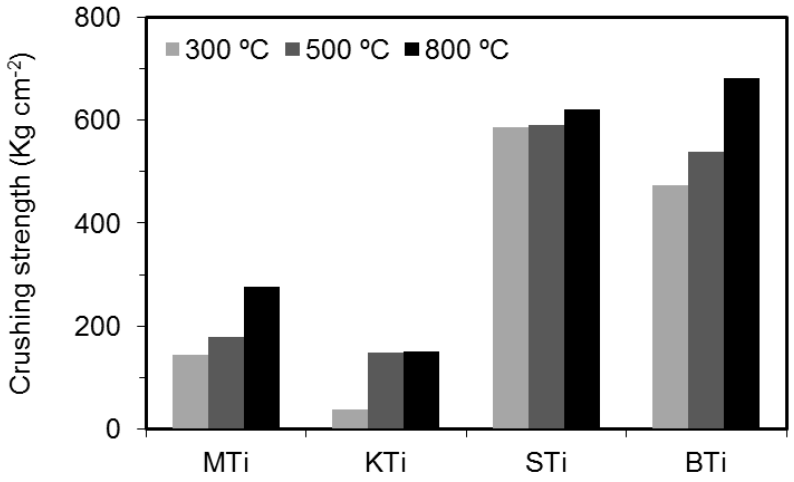

Figure 1. Crushing strength of silicate-TiO_2 plates calcined at different temperatures.

3.1.2 Optical properties

The UV-Vis absorption of the pure silicates is in general scarce, as previously reported for other clays such as motmorillonite [29], and only bentonite shows a small band (see **Figure S1A** Supporting Information). However, all hybrid materials absorb at wavelengths below 365 nm, like pure TiO_2-anatase, although in a smaller proportion that the pure material (**Figure S1B)**. The band gap energy was calculated by the so-called Tauc plot, a plot of the $(\alpha h\nu)^{1/\gamma}$ as a function of the $h\nu$ considering the power coefficient $\gamma = ½$ for direct allowed transition [42]. The band gap of the pure commercial TiO_2-anatase employed is not significantly modified in the composites by the presence of the silicate, with values of ca. 3.2 eV for all samples. Therefore, the APHs are expected to be photocatalytically active under UV-A irradiation. Moreover, since TiO_2 is incorporated during the kneading of the dough, the removal of the active phase from the immobilized catalyst by attrition during manipulation or operation that happens with coated materials is here minimized, and the adsorbent-semiconductor contact should be favored [31, 35] thus improving diffusional processes between components.

3.1.3 Textural and structural properties

Besides the role as binder for extrusion, the silicates are expected to play an important role in the adsorption and photocatalytic properties of the final material, related to their contribution to the physical and chemical properties of the composite. **Table 1** collects the main characterization results obtained for BTi, KTi, MTi, STi, and bare TiO_2 at different treatment temperatures.

Table 1. Textural and structural properties of the natural silicate-TiO_2 composites

Composites	Temp. ºC	Crystal size nm	MIP Area $m^2\ g^{-1}$	BET Area $m^2\ g^{-1}$	D_p[a] (max.) nm	D_p[b] (mean) nm	Pore volume $cm^3\ g^{-1}$
Ti*	300	9	-	250	5/20	7	0.38
	500	16	-	152	8/20	12	0.39
	800	47	-	63	-	-	0.29
	300	8	81	169	75	17	0.41
BTi	500	20	67	125	76	21	0.42
	800	60	24	22	90	56	0.34
	300	8	105	175	77	21	0.63
STi	500	13	95	136	87	24	0.62
	800	43	54	63	105	40	0.57
	300	10	78	130	70	25	0.55
KTi	500	20	60	73	80	34	0.54
	800	47	36	38	95	57	0.54
	300	14	70	170	230	24	0.48
MTi	500	17	50	65	250	34	0.45
	800	56	24	27	280	71	0.43

a Maximum of the pore diameter distribution

b Average pore diameter

* Data for TiO_2 powder obtained from N_2 adsorption isotherms only.

The textural properties can be also appreciated in **Figure 2,** that shows the pore size distribution of the extruded composites treated at 500 ºC (see **Figure S2** Supporting Information for the result obtained at different temperatures). All samples present mesoporosity, which is characteristic of the silicate arrangements. The textural properties of the bare TiO_2 used in our study have been previously reported [31, 34]. After thermal treatment at 300˚C, the TiO_2 powder has a BET area of 250 $m^2\ g^{-1}$ decreasing to 152 $m^2\ g^{-1}$ and 63 $m^2\ g^{-1}$ after calcination at 500˚C and 800˚C, respectively. The mean pore size of around 10 nm is due to the voids between titania aggregates. The incorporation of TiO_2 in the composites causes the formation of a sharp maximum in the big macropore range of the size distribution curves [43]. This effect can be clearly observed in **Figure S2D**, where the pore size distribution of bare sepiolite is shown for comparison. The formation of voids between TiO_2 aggregates or between silicate covered by TiO_2 particles could be the responsible of this macroporosity. STi, KTi and BTi have similar macropores of around 80 nm. However, the composites containing mordenite have significantly higher pores of 250 nm. In the case of the silicates with laminar morphology the silicate would be able, aided by the pressure applied for the extrusion, to partially fill the titania interparticular voids, reducing three times the size of the macropores. The mordenite zeolitic structure would limit the macropores filling. The total pore volume follows the

order STi > KTi > MTi > BTi. It must be remarked that the macropore volume of the bentonite-based composites is half of that of the other samples, and, accordingly, it has the higher crushing strength. Nevertheless, the fibrous structure of sepiolite also provides STi with a great crushing strength, indicating that both the morphology and type of layered structure determine the mechanical resistance of the composites. The total pore volume, mainly related to bigger pores, is not significantly affected by the temperature of the thermal treatment. During calcination, the smaller pores are lost due to the collapse of the mesoporous structure of the silicates. On the contrary, the wider pores increase slightly their size, because upon calcination titania particles suffer a sinterization process, *i.e.*, their size increases while the number of titania particles decreases, and as a consequence the size of the interparticle voids increases. **Figure S2** in the supporting information shows the porosity changes detected with the calcination at different temperatures. In general, the smaller mesopores observed in the samples calcined at 300 ºC disappear with the treatment at 500 ºC, and at 800 ºC the mesoporosity is also dramatically reduced. Thus, the porosity moves from a trimodal to a bimodal size distribution by effect of the calcination temperature. Accordingly, the surface area, which is related to the smaller pores, is reduced as the treatment temperature increases, as well as the difference between MIP and BET values.

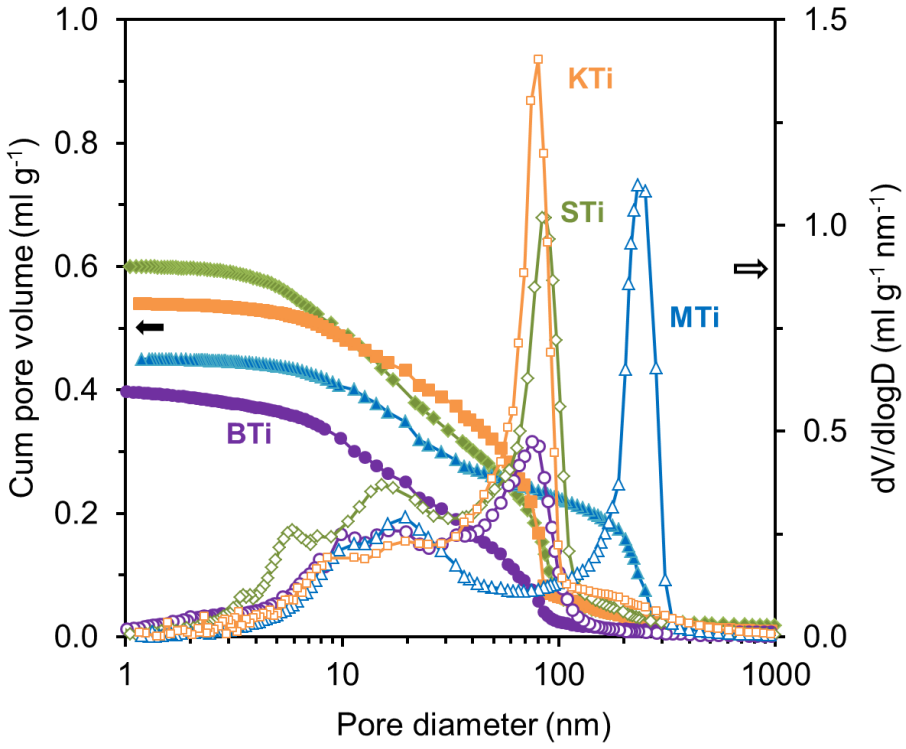

Figure 2. Cumulated pore volume (filled symbols) and pore size distribution (empty symbols) as obtained by combination of N_2 adsorption isotherms and MIP of silicate- TiO_2 samples treated at 500 ºC.

The silicates suffer different transformation processes during the thermal treatment of the extruded APHs related to the evolution of their inorganic framework. In order to complement the characterization to select the optimal calcination temperature for the APHs the thermogravimetric analyses of the natural silicates and titania employed as raw materials were performed and are presented in **Figure 3**. All of them show an endothermic weight loss between 80-150 ºC due to the elimination of physisorbed water and complete dihydroxylation above 800 ºC. At this temperature, the structure of the 2:1 silicates collapses irreversibly, leading to a significant reduction of the porosity of the composites.

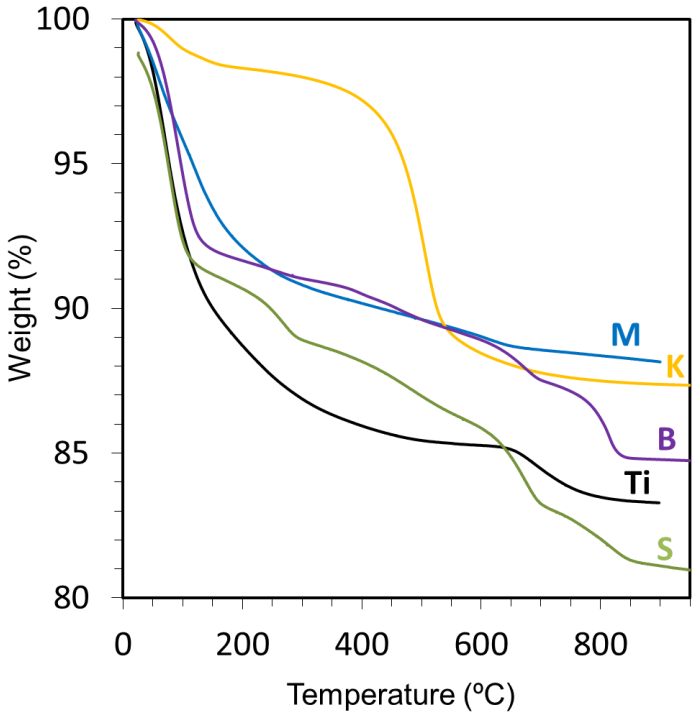

Figure 3. TGA curves for raw materials: M (mordenite), K (kaolinite), B (bentonite), S (sepiolite), Ti (titania).

Above 100 ºC sepiolite starts to lose zeolitic water and water of crystallization. The elimination of two of the water molecules coordinated to Mg at 300-350 ºC is associated with the reversible collapse of the internal structure into the anhydrous sepiolite form. Between 400-600 ºC the other two Mg-coordinated water molecules (constitutional water) are lost, and the material can no longer be rehydrated. The elimination of the hydroxyl groups takes place between 600-700 ºC, and the exothermic phase transformation to enstatite, which cannot be associated with a weight loss step, occurs at 800 ºC [44]. In the case of bentonite**,** the endothermic gradual weight loss between 400 and 700 ºC is due to the loss of the lattice OH^- groups in octahedral sheets of the silicate.

At 830 ºC the 2:1 layer structure completely collapses [45]. Kaolinite suffers a strong weight loss between 400-600 ºC, with a peak centered at 500 ºC in the DTA curve. According to the literature, the dehydroxylation of the single layer of water between the 1:1 silicate layers with the formation of metakaolinite, a semicrystalline phase, takes place at this temperature range [25]. Mordenite suffers a moderate weight loss of around 10 % during the thermal treatment. The process is assigned to the elimination of the hydroxyl groups from the surface up to 600 ºC, and isolated hydroxyl groups at higher temperatures [46]. The TG analyses indicate that, besides maintaining most of the porous structure, a temperature of 500 ˚C, allows the materials to preserve the silicate structure hydroxylated, which is adequate to carry out the photocatalytic reaction. While the mechanical strength of the composites increases when they are heat treated at 800˚C, the silicate structure collapses at such high temperature, causing a reduction of the pore volume and surface area and the removal of –OH structural groups.

The differences in the crystalline structure of the APHs have been investigated by XRD. The patterns of the composites treated at 500 ºC are depicted in **Figure 4**. They contain the diffraction peaks of the corresponding silicates and those of anatase-TiO_2, but the presence of other crystalline phases of TiO_2 is discarded. Therefore, the incorporation of the titania into the silicate matrix delays the rutilation temperature: contrary to what usually happens with pure TiO_2, in all the APHs practically no rutile is observed up to 500 ºC, and it can only be envisaged after treatment at 800 ºC, as previous works also found for TiO_2-sepiolite composites [35].

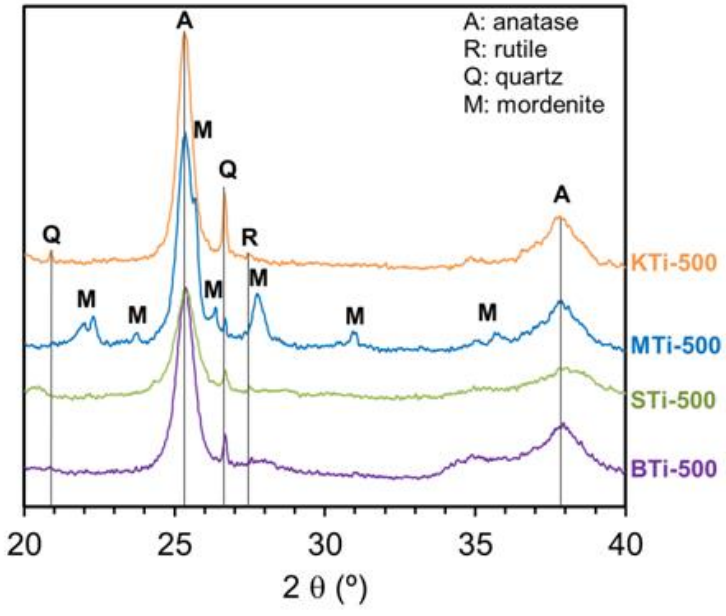

Figure 4. XRD pattern of the silicate-TiO_2 composites treated at 500 ºC.

The size of the TiO_2-anatase crystalline domains in the hybrids, as estimated by the Scherer's equation, significantly increases with the temperature of the heat treatment applied, from around 10 nm for 300 ºC to, at the highest temperature, ca. 45 nm for STi and KTi (similarly to bare TiO_2) and to ca. 60 nm for BTi and MTi (see **Table 1**). The evolution of the TiO_2-anatase diffraction peaks with the temperature in the APHs is clarified in the **Figure S3** (Supporting Information).

Finally, ICP analysis were performed to confirm the titania content in the composites and identify the main impurities. **Table 2** contains the mean bulk composition of the plate-shaped materials revealed by ICP analysis. The values are similar to EDX results, calculated as weight per cent of inorganic oxide. The amount of titania is close to the theoretical value of 50 wt.%. Unlike most bentonites which present aluminum and silicon as dominant elements, the bentonite employed in this study is a magnesium-rich material with a small amount of alumina. The presence of Mg in the aluminosilicates used in this work, kaolinite and mordenite, is negligible. Sodium, calcium, potassium and iron are the other elements identified in the analyses of the samples under study. These elements are usually present in natural silicates.

Table 2. Chemical composition (wt.%) obtained by ICP analysis

	TiO_2	SiO_2	MgO	Al_2O_3	Na_2O	CaO	K_2O	Fe_2O_3
BTi-500	46.2	29.8	16.8	2.3	2.5	0.6	0.3	1.5
STi-500	45.9	33.7	12.5	3.0	0.5	2.1	0.7	1.7
KTi-500	46.8	28.2	0.2	21.8	0.3	0.1	0.9	1.8
MTi-500	45.1	39.1	0.6	7.2	3.3	1.3	1.5	1.8

3.1.4 Morphological properties

Microscopy analyses reveal the morphological differences of the samples under study. ¡Error! No se encuentra el origen de la referencia. **Figure 5** left and right depict scanning and transmission electron micrographs, respectively, for the BTi, KTi, and MTi samples treated at 500 ºC. In the case of SEM study ceramic plate fragments were analyzed, and thus the real distribution of TiO_2 in the silicate was observed. However, TEM micrographs was performed with ground particles. A coral-like structure is observed for the bentonite-based sample (**Figure 5A left**), where spherically agglomerated particles with mean diameter of 800 nm are cross-linked in a closed porous structure. These observations are consistent with the textural and mechanical properties of these samples

and with previous SEM characterization reported in literature [19]. BM-500 presents a layered structure similar to that reported for fresh bentonite [47], but with large clusters of titania nanoparticles (dark areas in **Figure 5A right**) along with smaller aggregates of 80-100 nm. TiO_2 incorporation does not seem to promote interlayer separation as previously reported for sepiolite fibres [43]. The morphology of the sepiolite-titania composite has been previously reported in the literature. The structure is characterized by bundles of fibers of around 0.2 μm diameter and up to 2.4 μm length covered by TiO_2 particles and aggregates of different size [31].

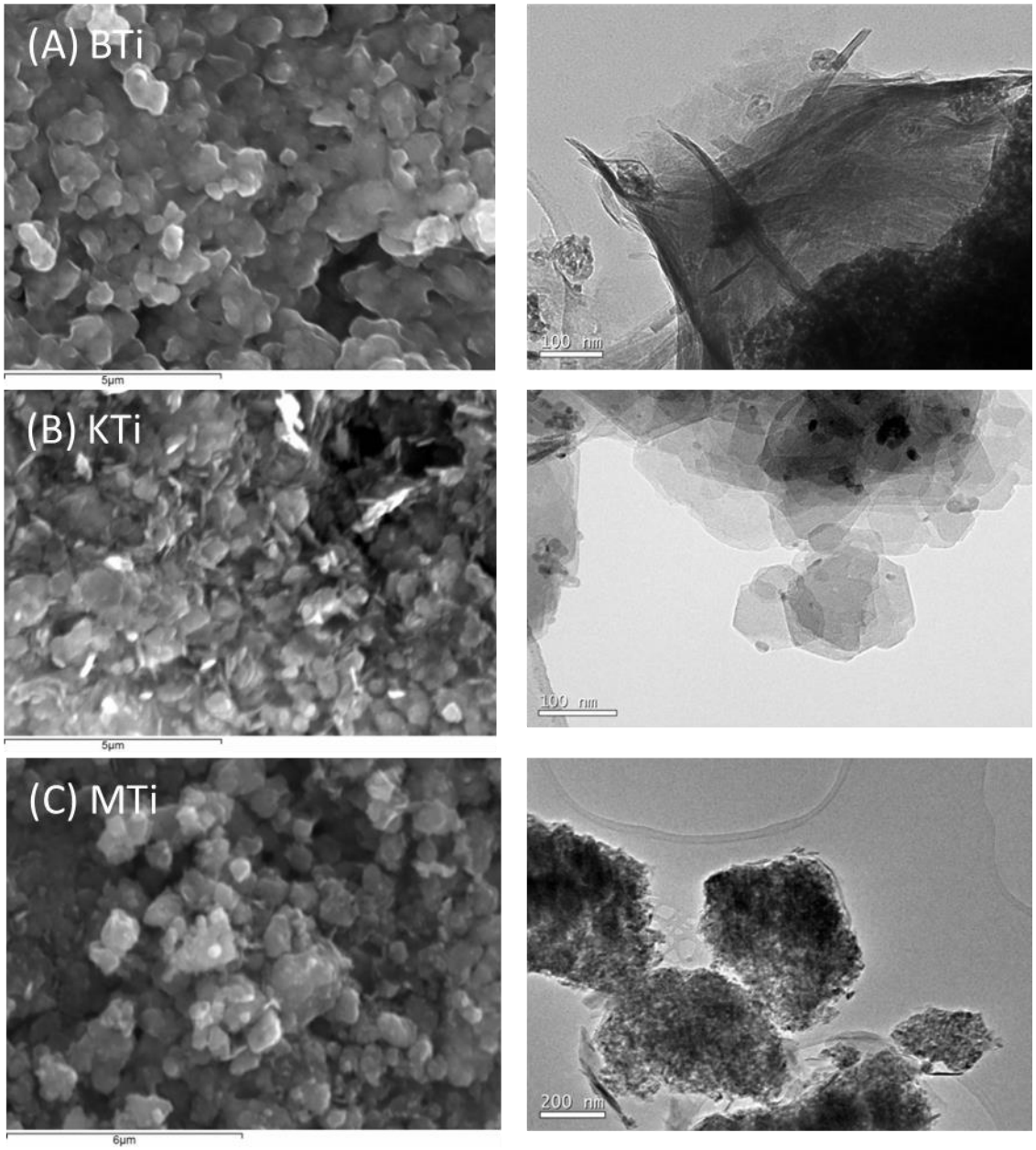

Figure 5. SEM (left) and TEM (right) micrographs of silicate-TiO_2 composites: A) BTi-500, B) KTi-500, and C) MTi-500composites.

The kaolinite-based materials show the typical phyllosilicate laminar structure of kaolinite, the long axis of the six-sided particles ranging between 100-500 nm, with titania particles decorating the layers (**Figure 5B**) [48]. The distribution of TiO_2 paricles on this silicate is homogeneous, without formation of TiO_2 aggregates. A completely different morphology is observed for mordenite-based composites, with mordenite aggregates covered by titania particles and a more porous structure (¡Error! No se encuentra el origen de la referencia.**Figure 5C**) [49]. MTi-500 is characterized by TiO_2 particles smaller than 20 nm located on the external surface of the mordenite granules, with size between 200-800 nm [50]. The commercial TiO_2 was also characterized by SEM (Figure S4, supporting information). TiO_2 nanoparticles of 10-20 nm mean size tend to form irregular clusters of ca. 1.0 μm. Thus, the incorporation of the silicate promotes the dispersion of the titania particles, decreasing the aggregates size to 100-200 nm. EDX general mapping analyses reveal that titanium and silicon are homogeneously distributed in all the composites, without titania- or silica-enriched areas.

3.1.5 HCHO dynamic adsorption

Table 3 reports the formaldehyde adsorption amounts of the raw materials and the composites, studied at dynamic conditions. Among the constituents of the silicate-TiO_2 composites, TiO_2 displays by far the highest dynamic adsorption capacity of 3.40 $mmol_{HCHO}$ g^{-1}. This value is much higher than the adsorption capacity of mordenite, the best performing of the natural silicates under study, as shown in **Table 3**, with 0.62 mmol of adsorbed HCHO per gram of material. Similarly, TiO_2-P25 has greater adsorption capacity for formaldehyde than conventional adsorbents such as activated carbon [51]. However, the adsorption capacity of benchmark TiO_2-P25 for HCHO is only 0.59 mmol g^{-1} when evaluated under the experimental conditions reported in this work, around six times lower than the adsorption capacity of TiO_2–G5. Different aspects could be considered to explain this big difference, such as the presence of TiO_2-rutile (20%) and the low surface area of TiO_2-P25 (45 m^2 g^{-1} vs. 321 m^2 g^{-1} of G5). The lower affinity for the aldehyde of the silicates, in spite of their relatively high surface area, would be explained in part by the Lewis acidic character of titania, while silica does not have acid sites [52]. It has been accepted that in ionic oxide surfaces HCHO adsorption takes place

via dioxymethylene formation. A lone pair donation from the oxygen of the carbonyl group to Lewis acid sites, such as Ti cations, increases the electrophilicity, favoring the nucleophilic attack from surface oxygen to the carbonyl group [53]. The dioxymethylene species formed may then undergo a Cannizzaro-type disproportionation, giving rise to methoxy groups and formate species [54].

Table 3. Surface properties of the raw materials and composites after treatment at 500 ºC

Composition	ZPC	X_{TiO2}	Dynamic HCHO adsorption, mmol g^{-1}		
	pH	mol %	Measured	Estimated$_{50\%}$ [a]	EstimatedX_{TiO2} [b]
Ti	6.3	100	3.40	-	-
B	2.1	0	0.10	-	-
S	2.2	0	0.02	-	-
K	2.3	0	0.01	-	-
M	<1	0	0.62	-	-
BTi	2.6	16	0.22	1.75	0.64
STi	2.5	7	0.21	1.81	0.27
KTi	3.3	27	0.29	1.70	0.91
MTi	2.4	34	0.98	2.01	1.56

[a] Adsorption expected for a material containing equal amounts of TiO_2 and clay

[b] Adsorption expected according the molar fraction of TiO_2 in the surface calculated by Eq. 6.

The adsorption capacity of the hybrids lies between that of the individual components; thus MTi exhibits the highest capacity for HCHO adsorption. However, the values expected taking into account that the material contains equal amounts of TiO_2 and silicate (estimated$_{50\%}$ in **Table 3**) are much higher that the values actually measured. Apparently, a fraction of the adsorption capacity of TiO_2 is lost in the composite. One explanation would be a more reduced acidity of the titanium cations in the mixture, but more probably is due to the fact that a fraction of the titania active sites is not available for HCHO adsorption in the composite.

Figure 6 shows the influence of the calcination temperature and the BET area on the amount of formaldehyde adsorbed, for the hybrid materials collected in Table 1. For a given composition, the treatment temperature affects the adsorption capacity (see **Figure 6A)** due to changes in porosity, surface area and size of TiO_2 crystalline domains. Only MTi presents similar adsorption at 300 and 500 ºC, despite the significant difference of surface area. The differences among silicates are consequence of other factors. Mordenitic hybrids display much higher adsorption for the same BET area (**Figure 6B**), and this must be explained by the chemical, structural and morphological differences. The

higher adsorption capacity of the zeolitic component, the bigger macropores, but especially the higher fraction of TiO_2 on the surface compared to the other composites must favor the adsorption of the aldehyde. KTi adsorption is similar to BTi and STi samples when treated at the same temperature, despite the fact that the BET area of the former is significantly lower.

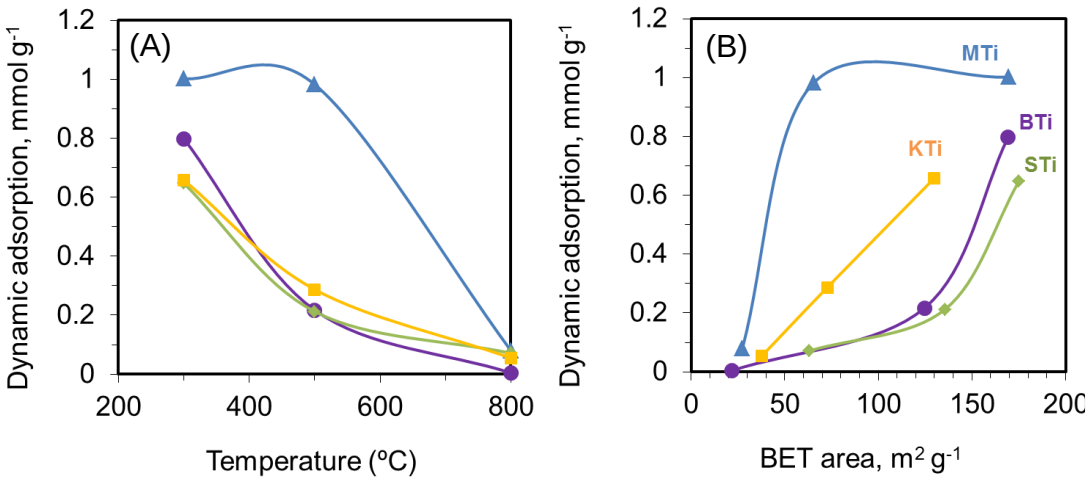

Figure 6. HCHO dynamic adsorption of silicate-TiO_2 hybrids as a function of (A) temperature and (B) BET area obtained at different treatment temperatures. Operating conditions: Air flow rate = 0.7 L min^{-1}, [HCHO] = 15 ppmv, T = 35 ºC.

3.1.6 TiO_2 distribution into the silicate

The isoelectric point of hybrid materials gives information on the surface properties and can be used to estimate the apparent molar fraction of exposed TiO_2 (X_{Ti}) substituting the isoelectric point (IEP) of the components in the modified Park's equation [55, 56]:

$$IEP_{YTi} = (1 - X_{Ti})IEP_Y + X_{Ti}IEP_{Ti} \qquad Eq.\ 1$$

Therefore, in order to explain the adsorption behavior of the composites, electrophoretic migration measurements and Eq. 1 were used to estimate X_{Ti} for the clay-TiO_2 hybrids. The results are included in **Table 3**. The ZPC, which depends on the charges on the solid surface in contact with the aqueous media, indicates that bulk TiO_2 content is higher than surface TiO_2. The estimated fraction of exposed titania on the surface of the particles is quite low and follows the order MTi > KTi >> BTi > STi, which is coherent with the trend of the adsorption capacity and with the morphological characterization. However, the measured HCHO adsorption capacity is even below the value calculated taking into account the exposed TiO_2 (estimated$_{XTiO2}$ in **Table 3**). Important diffusional limitations

due to a different arrangement between silicate and titania, including the silicate in the titania interparticular voids, could restrict further the adsorption capacity.

3.2 HCHO photocatalytic degradation

Some silicates, such as montmorillonite [57] or kaolinite [58], have been reported to show catalytic activity under UV irradiation for degradation of gas-phase organic pollutants, for instance decabromodiphenyl ether and toluene, which has been attributed to the charge transfer between the mineral and the adsorbed species or to generation of radicals on the surface of the clay. The silicates under study do not show any reactivity for HCHO removal under irradiation, with the only exception of bentonite, the one that shows some radiation absorption (see Figure S1A), which reduced the concentration of HCHO by 8%. All the silicate-TiO_2 hybrids prepared, however, present high photocatalytic activity. The mechanism of formaldehyde photocatalytic degradation can be described by the following steps [59]:

$$HCHO + \cdot OH \rightarrow \cdot CHO + H_2O \qquad \textit{Eq. 2}$$

$$\cdot CHO + \cdot OH \rightarrow HCOOH \quad \text{or}$$

$$\cdot CHO + \cdot O_2^- \rightarrow CHO_3^- \xrightarrow{+H^+} HCOOOH \xrightarrow{+HCHO} 2HCOOH \qquad \textit{Eq. 3}$$

$$HCOOH \rightarrow H^+ + HCOO^- \qquad \textit{Eq. 4}$$

$$HCOO^- + \cdot OH \rightarrow H_2O + \cdot CO_2^- \quad \text{or}$$

$$HCOO^- + h^+ \rightarrow H^+ + \cdot CO_2^- \qquad \textit{Eq. 5}$$

$$\cdot CO_2^- \xrightarrow{\cdot OH,\ h^+} CO_2 \qquad \textit{Eq. 6}$$

Thus, formic acid can be generated besides carbon dioxide. The carbon balance indicates that in all cases the formaldehyde removed was completely mineralized. Accordingly, no partial oxidation byproducts, such as formic acid [51] or CO [60], have been detected in the gas phase.

3.2.1 Effect of the calcination temperature

The effect of the heat treatment on the photocatalytic activity is similar for all silicates. The composites treated at 300 ºC or 500 ºC achieve total mineralization of the pollutant at the highest residence time tested; with increasing flow rates the residence time is

reduced, leading to a decrease of the conversion values, especially at the highest treatment temperature and for STi and BTi composites (**Figure 7)**.The comparison of the photocatalytic activity of the hybrids heat treated at 500ºC indicates the best performance of the mordenitic and kaolinitic based materials compared to bentonite and sepiolite composites. The performance of the samples treated at 800 ºC is dramatically worse, the conversion values drop below 20%. There is not a direct correlation between the photocatalytic degradation of HCHO and the surface area values of **Table 1**, because the dependence of the BET area on the temperature is approximately linear, so additional factors have to be taken into account, such as the collapse of the silicates structure and the reduction of the porosity at the highest heat treatment temperature, as shown by the TGand MIP analyses. The dehydroxylation of the surface may reduce the formation of OH radicals during the photocatalytic process, havig a strong influence on the photoefficiency.

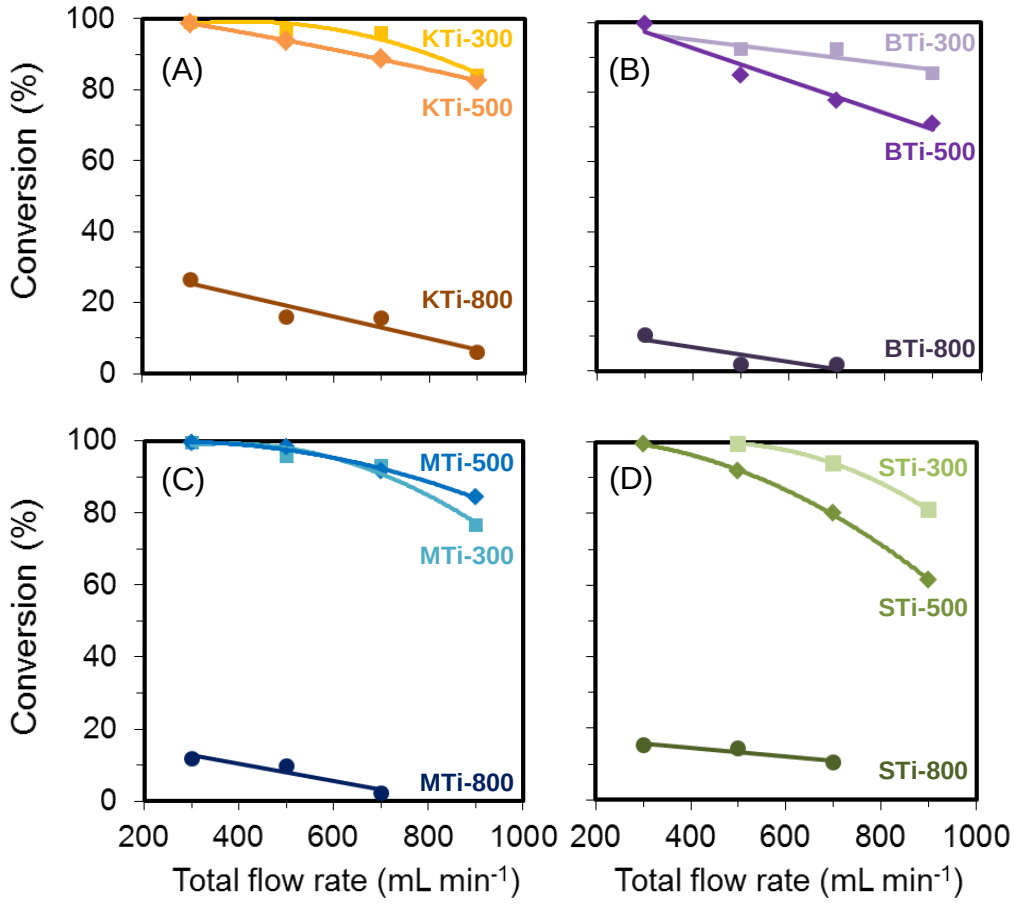

Figure 7. Effect of the composites treatment temperature on the HCHO photodegradation efficiency for: (A) KTi, (B) BTi, (C) MTi and (D) STi silicate-TiO_2 APHs.

3.2.2 Influence of the TiO_2 crystal size and HCHO adsorption

Another factor to be considered is the growth of the crystalline domains of TiO_2, with mean sizes around 4-5 times higher at 800 ºC than those obtained at 300 ºC, associated to poor titania dispersion and a faster electron-hole recombination. **Figure 8** shows the influence of the TiO_2 crystal size and the HCHO adsorption on the photocatalytic conversion for the different silicate-TiO_2 composites heat treated between 300-800ºC. The TiO_2 crystal size seems to be a key factor for the photocatalytic activity, as **Figure 8A** reflects. Thus, the efficiency can be increased by improving the dispersion of TiO_2 particles, which reduces the diffusion length. This observation is in agreement with previous studies on hybrid photocatalysts [61]. Not only the adsorption, but also the diffusion of the adsorbed pollutant towards the photocatalytically active sites determines the decomposition rate in APHs [62]. It is worth noting that, in the operating conditions studied, the reaction rate is limited by the adsorption step only at low adsorption capacity, below 0.1 mmol g^{-1}. Above this value, the conversion obtained at a fixed gas flow is independent of the HCHO adsorption capacity. For instance, at 700 mL min^{-1} HCHO conversion is between 80-100% (**Figure 8B**).

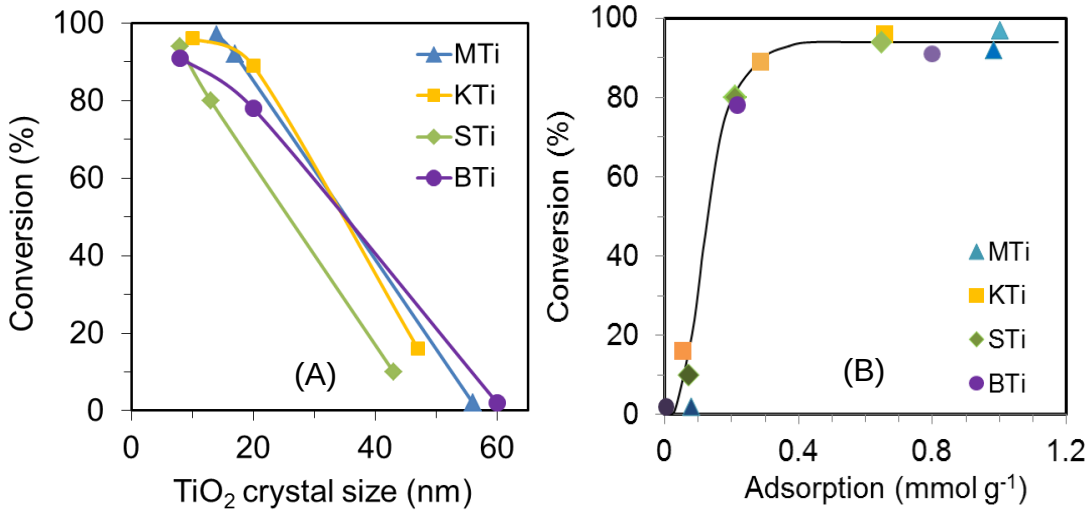

Figure 8. HCHO photocatalytic degradation over silicate-TiO_2 hybrids calcined at different temperatures as a function of (A) crystal size of anatase-TiO_2 and (B) adsorption capacity. Operating conditions: Air flow rate = 0.7 L min^{-1}, [HCHO] = 15 ppm_v, T = 35 ºC.

3.2.3 Effect of the fraction of TiO_2 exposed

The molar fraction of TiO_2 that is available in the surface of the hybrid materials depends on the silicate used as binder/adsorbent, as indicated in Table 3. This can be better observed in **Figure 9A**, where the molar fraction of TiO_2 on the surface calculated by electrophoretic migration is plotted *vs.* the weight % in the bulk for several silicates and silicate-to-semiconductor ratios. The adsorption capacity and photocatalytic activity of the 50 wt.% composites are plotted in **Figure 9B**, where it can be inferred that both properties are not directly correlated, but are affected by the exposed TiO_2 in the same direction. Since HCHO is preferably adsorbed on TiO_2, it can be concluded that the fraction of TiO_2 exposed on the surface is a key factor for the APHs, because it influences both adsorption and photocatalytic oxidation processes. Despite of this fact, the advantage of the composites over pure TiO_2 remains clear, not only due to the possibility of shaping the photocatalyst, but also to the synergy observed.

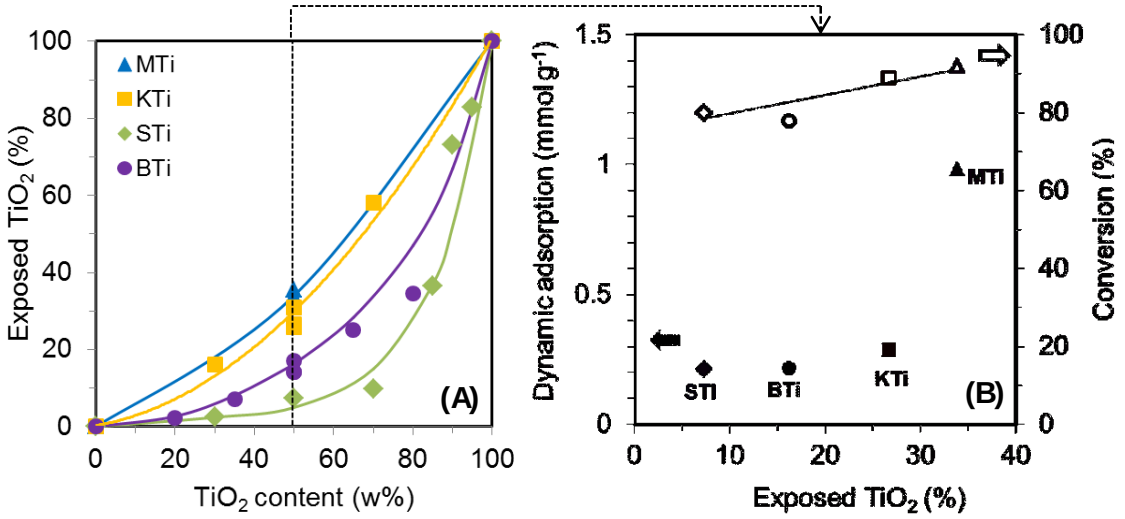

Figure 9. (A) Exposed TiO_2 as a function of the TiO_2 content in the composites. (B) Formaldehyde adsorption (left, filled symbols) and photocatalytic degradation (right, void symbols) for silicate-TiO_2 composites as a function of the exposed TiO_2 in the surface of the particles estimated by electrophoretic migration. All samples are treated at 500 ºC.

Formaldehyde conversion with pure TiO_2 at a total gas flow of 900 mL min^{-1} was 86 %, similar to the values obtained with KTi-500 and MTi-500 composites. However, for an accurate comparison the actual TiO_2 content should be considered. Thus, reaction rates normalized per gram of TiO_2 were calculated, for natural silicate–TiO_2 hybrids and TiO_2

at two different total gas flows, 500 and 900 mL min^{-1} (**Figure 10**). As shown in this figure, the normalized reaction rates, clearly indicate that the incorporation of titania into the silicate matrix favors the gas phase removal of HCHO. The normalized activity follows the sequence: MTi > KTi > STi > BTi > TiO_2. The results obtained in this study reveal that silicate-based composites, especially with mordenite and kaolinite, have excellent photocatalytic properties compared to benchmark titania. The nature of the silicate plays a relevant role to control and improve TiO_2 dispersion and its exposed fraction at the surface, as observed by SEM and electrophoretic migration measurements. Moreover, the silicates have a high specific surface area and, in general, contribute to the adsorption properties. This feature might increase the concentration of the pollutant in the vicinity of the titania active sites, improving the reaction rate. As a consequence, TiO_2 photocatalytic activity for the degradation of HCHO is promoted. The silicates studied in this work are suitable substrates to anchor TiO_2 particles and prepare low-cost easy-to-handle ceramic structures.

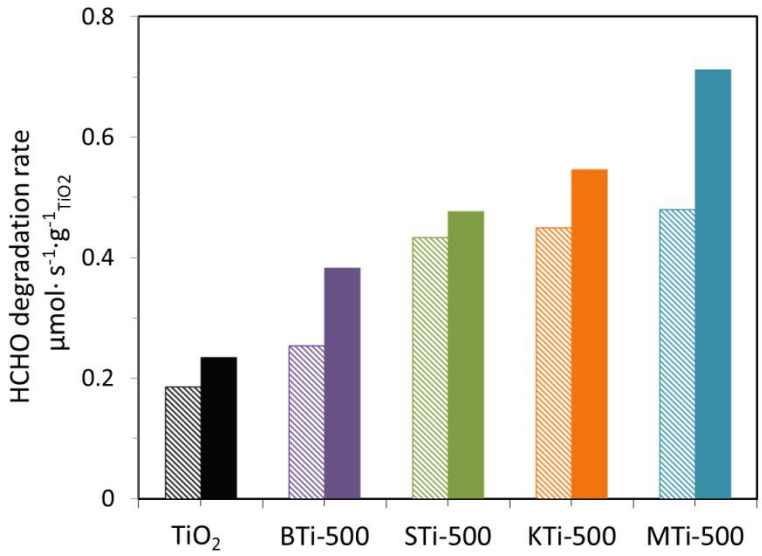

Figure 10. HCHO degradation rate at flow rates of 500 mL min^{-1} (hatched bars) and 900 mL min^{-1} (filled bars) for the silicate-TiO_2 hybrids and commercial TiO_2, treated at 500˚C.

Conclusions

Plate-shaped ceramic APHs (adsorbent-photocatalyst hybrids) were extruded using doughs with adequate plasticity prepared by mechanical mixture of commercial powdered constituents with water. This preparation method meets the simplicity and economy

criteria of industrial processes, which are not fulfilled by more complex lab scale methods (pillarization, sol-gel, etc.). The choice of the adequate binder for photocatalytic applications of hybrid materials should be taken by considering several key aspects such as its interaction with the semiconductor phase and the adsorption ability towards the targeted pollutants and reaction products. The commercial TiO_2 selected for this study is a very active material for HCHO photodegradation; however, it cannot be shaped into easily handled structures. Among the natural silicates under study, mordenite presents the higher HCHO adsorption capacity. The adsorption ability of the composites depends on the number of available adsorption sites and their chemical properties, which are in turn controlled by its specific surface area and chemical composition. The heat treatment produces structural modifications of the constituents but is not enough to develop chemical interactions between both type of phases. Thermal treatments at high temperatures reduce the mesoporosity and dispersion of titania, as a consequence, the adsorption ability of the silicate-TiO_2 photocatalysts. TiO_2 acts both as adsorbent and as photocatalyst phase for the elimination of gaseous formaldehyde. Therefore, in order to optimize HCHO adsorption and conversion efficiency, TiO_2 content and dispersion in natural silicate-semiconductor composites should be increased. Nevertheless, the photocatalytic activity depends not only on the adsorption property of reactants and products on the composites, but also on their diffusion and on the number of exposed photocatalytically active TiO_2 sites. All the silicate-TiO_2 composites developed in this study improve the HCHO degradation rate of commercial TiO_2, especially those based on mordenite and kaolinite structures, which maximize the fraction of TiO_2 exposed at the surface of the silicate.

Acknowledgements

The authors would like to express their thanks to Prof. F.J. Gil-Llambías for fruitful discussions on ZPC measurements and F.J. García-García for TEM analysis. Dr. R. Portela and Dr. S. Suárez are grateful to the Spanish Ministry of Economy and Competitiveness (Spain) for Juan de la Cierva and Ramón Cajal (RyC2007-01123) contracts, respectively. This research was funded by the project INNOFOTO (CTM2011-25093 MINECO-Spain) and the project Ref.: 1130749 (Fondecyt-Chile).

Bibliography

[1] M.R. Hoffmann, S.T. Martin, W.Y. Choi, D.W. Bahnemann, Environmental applications of semiconductor photocatalysis, Chem. Rev., 95 (1995) 69-96.

[2] Y. Ohko, K. Hashimoto, A. Fujishima, Kinetics of Photocatalytic Reactions under Extremely Low-Intensity UV Illumination on Titanium Dioxide Thin Films, J. Phys. Chem. A, 101 (1997) 8057-8062.

[3] D.M. Blake, Bibliography of Work on the Photocatalytic Removal of Harzadous Compounds from Water and Air and Updates number 1, 2, 3 and 4, National Renewable Energy Lab. Golden, CO (United States), 1994, 1995, 1996, 1999 and 2001.

[4] R. Portela, M.D. Hernández-Alonso, Environmental applications of photocatalysis, in: J.M. Coronado, M.D. Hernandez-Alonso, F. Fresno, R. Portela (Eds.) Design of advanced photocatalytic materials for energy and environmental applications, Springer-Verlag, London, 2013, pp. 35-66.

[5] M. Maroni, B. Seifert, T. Lindvall, Indoor Air Quality: A Comprehensive Reference Book, Elsevier, Amsterdam, 1995.

[6] P. Chin, L.P. Yang, D.F. Ollis, Formaldehyde removal from air via a rotating adsorbent combined with a photocatalyst reactor: Kinetic modeling, J. Catal., 237 (2006) 29-37.

[7] D. Vildozo, R. Portela, C. Ferronato, J.-M. Chovelon, Photocatalytic oxidation of 2-propanol/toluene binary mixtures at indoor air concentration levels, Appl. Catal., B, 107 (2011) 347-354.

[8] T. Van Gerven, G. Mul, J. Moulijn, A. Stankiewicz, A review of intensification of photocatalytic processes, Chemical Engineering and Processing: Process Intensification, 46 (2007) 781-789.

[9] S. Suárez, Immobilised photocatalysts, in: J.M. Coronado, F. Fresno, M.D. Hernández-Alonso, R. Portela (Eds.) Design of Advanced Photocatalytic Materials for Energy and Environmental Applications, Springer London, 2013, pp. 245-267.

[10] F. Fresno, R. Portela, S. Suarez, J.M. Coronado, Photocatalytic materials: recent achievements and near future trends, J. Mater. Chem. A, 2 (2014) 2863.

[11] K. Suzuki, Photocatalytic air purification on TiO_2 coated honeycomb support, in: D.F.Ollis, H.Al-Ekabi (Eds.) Photocatalytic Purification and Treatment of Water and Air, Elsevier Science Publishers B.V.1993, pp. 421-434.

[12] M.L. Sauer, D.F. Ollis, Acetone oxidation in a photocatalytic monolith reactor, J. Catal., 149 (1994) 81-91.
[13] J. Blanco, P. Avila, A. Bahamonde, E. Alvarez, B. Sánchez, M. Romero, Photocatalytic destruction of toluene and xylene at gas phase on a titania based monolithic catalyst, Catal. Today, 29 (1996) 437-442.
[14] P. Avila, A. Bahamonde, J. Blanco, B. Sánchez, A.I. Cardona, M. Romero, Gas-phase photo-assisted mineralization of volatile organic compounds by monolithic titania catalysts, Appl. Catal. B, 17 (1998) 75-88.
[15] B. Sánchez, A.I. Cardona, M. Romero, P. Avila, A. Bahamonde, Influence of temperature on gas-phase photo-assisted mineralization of TCE using tubular and monolithic catalysts, Catal. Today, 54 (1999) 369-377.
[16] H. Yoneyama, T. Torimoto, Titanium dioxide/adsorbent hybrid photocatalysis for photodestruction of organic substances of dilute concentrations, Catal. Today, 58 (2000) 133-140.
[17] N. Bouazza, M.A. Lillo-Ródenas, A. Linares-Solano, Enhancement of the photocatalytic activity of pelletized TiO_2 for the oxidation of propene at low concentration, Appl. Catal. B, 77 (2008) 284-293.
[18] J. Mo, Y. Zhang, Q. Xu, R. Yang, Effect of TiO_2/adsorbent hybrid photocatalysts for toluene decomposition in gas phase, J. Hazard. Mater., 168 (2009) 276-281.
[19] J. Chen, G. Li, Z. He, T. An, Adsorption and degradation of model volatile organic compounds by a combined titania–montmorillonite–silica photocatalyst, J. Hazard. Mater., 190 (2011) 416-423.
[20] R. Leary, A. Westwood, Carbonaceous nanomaterials for the enhancement of TiO_2 photocatalysis, Carbon, 49 (2011) 741-772.
[21] Y. Kuwahara, H. Yamashita, Efficient photocatalytic degradation of organics diluted in water and air using TiO2 designed with zeolites and mesoporous silica materials, J. Mater. Chem., 21 (2011) 2407-2416.
[22] L. Zou, Y. Luo, M. Hooper, E. Hu, Removal of VOCs by photocatalysis process using adsorption enhanced TiO2–SiO2 catalyst, Chem. Eng. Process., 45 (2006) 959-964.
[23] K. Rajeshwar, W. Chanmanee, Bioinspired photocatalyst assemblies for environmental remediation, Electrochimica Acta, 84 (2012) 96-102.
[24] C.J. Liao, S.L. Kuo, Inactivation of bacteria by kaolinite photocatalysts in water, Environ. Eng. Sci., 25 (2008) 33-42.

[25] M.N. Chong, V. Vimonses, S. Lei, B. Jin, C. Chow, C. Saint, Synthesis and characterisation of novel titania impregnated kaolinite nano-photocatalyst, Microporous Mesoporous Mater., 117 (2009) 233-242.
[26] P. Pichat, H. Khalaf, D. Tabet, M. Houari, M. Saidi, Ti-montmorillonite as photocatalyst to remove 4-chlorophenol in water and methanol in air, Environ. Chem. Lett., 2 (2005) 191-194.
[27] J. Ménesi, L. Körösi, É. Bazsó, V. Zöllmer, A. Richardt, I. Dékány, Photocatalytic oxidation of organic pollutants on titania–clay composites, Chemosphere, 70 (2008) 538-542.
[28] P. Aranda, R. Kun, M.A. Martín-Luengo, S. Letaïef, I. Dékány, E. Ruiz-Hitzky, Titania−Sepiolite Nanocomposites Prepared by a Surfactant Templating Colloidal Route, Chem. Mater., 20 (2007) 84-91.
[29] C. Ooka, S. Akita, Y. Ohashi, T. Horiuchi, K. Suzuki, S.-i. Komai, H. Yoshida, T. Hattori, Crystallization of hydrothermally treated TiO_2 pillars in pillared montmorillonite for improvement of the photocatalytic activity, J. Mater. Chem., 9 (1999) 2943-2952.
[30] S. Letaief, E. Ruiz-Hitzky, Silica-clay nanocomposites, Chem. Commun., (2003) 2996-2997.
[31] S. Suárez, J.M. Coronado, R. Portela, J.C. Martín, M. Yates, P. Ávila, B. Sánchez, On the preparation of TiO_2-sepiolite hybrid materials for the photocatalytic degradation of TCE: influence of TiO_2 distribution in the mineralization., Environ. Sci. Technol., 42 (2008) 5892-5896.
[32] S.B. Rasmussen, R. Portela, S. Suárez, J.M. Coronado, M.L. Rojas-Cervantes, P. Avila, B. Sánchez, Hybrid TiO_2/SiMgOx Composite for Combined Chemisorption and Photocatalytic Elimination of Gaseous H2S, Ind. Eng. Chem. Res., 49 (2010) 6685–6690.
[33] R. Portela, R.F. Tessinari, S. Suárez, S.B. Rasmussen, M.D. Hernández-Alonso, M.C. Canela, P. Ávila, B. Sánchez, Photocatalysis for continuous air purification in wastewater treatment plants: from lab to reality, Environ. Sci. Technol., 46 (2012) 5040-5048.
[34] S. Suárez, T.L.R. Hewer, R. Portela, M.D. Hernandez-Alonso, R.S. Freire, B. Sanchez, Behaviour of TiO_2-SiMgOx hybrid composites on the solar photocatalytic degradation of polluted air, Appl. Catal., B, 101 (2011) 176-182.
[35] T.L.R. Hewer, S. Suárez, J.M. Coronado, R. Portela, P. Avila, B. Sanchez, Hybrid photocatalysts for the degradation of trichloroethylene in air, Catal. Today, 13 (2009) 302-308

[36] A. Bahamonde, F. Mohino, M. Rebollar, M. Yates, P. Avila, S. Mendioroz, Pillared clay and zirconia-based monolithic catalysts for selective catalytic reduction of nitric oxide by methane, Catal. Today, 69 (2001) 233-239.

[37] N.R. Sanabria, P. Ávila, M. Yates, S.B. Rasmussen, R. Molina, S. Moreno, Mechanical and textural properties of extruded materials manufactured with AlFe and AlCeFe pillared bentonites, Appl. Clay Sci., 47 (2010) 283-289.

[38] E. García-Romero, M. Suárez, V. López-Acevedo, J.A. López-García, M. Regueiro, The *"Los Murcianos"* zeolite deposit (San José, Almería) Geo-Temas, 10 (2008) ISSN: 1567-5172.

[39] A. Álvarez, Sepiolite: properties and uses, in: A. Singer, E. Galán (Eds.) Palygorskite-sepiolite occurrences, genesis, and uses Elsevier, Amsterdam, 1984, pp. 253-289.

[40] ASTM, D 4179 - Standard Test Method for Single Pellet Crush Strength of Formed Catalyst Shapes, 2001.

[41] G.J. Hutchings, Crusing strength as a diagnostic test for potocatalysis, J. Chem. Technol. Biotechnol., 36 (1986) 255-258.

[42] J. Tauc, Absorption edge and internal electric field in amorphous semiconductor, Mater. Res. Bull., 5 (1970) 721-729.

[43] P. Avila, J. Blanco, A. Bahamonde, J.M. Palacios, C. Barthelemy, Influence of the binder on the properties of catalysts based on titanium-vanadium oxides, J. Mater. Sci., 28 (1993) 4113-4118.

[44] H. Nagata, S. Shimoda, T. Sudo, On dehydration of bound water of sepiolite, Clays Clay Miner., 22 (1974) 285-293.

[45] J.-H. Choy, J.-H. Park, J.-B. Yoon, Multilayered SiO_2/TiO_2 Nanosol Particles in Two-Dimensional Aluminosilicate Catalyst−Support, J. Phys. Chem. B, 102 (1998) 5991-5995.

[46] O. Korkuna, R. Leboda, J. Skubiszewska-Zie¸ba, T. Vrublevs'ka, V.M. Gun'ko, J. Ryczkowski, Structural and physicochemical properties of natural zeolites: clinoptilolite and mordenite, Microporous Mesoporous Mater., 87 (2006) 243-254.

[47] A. Rinaldi, J. Zhang, J. Mizera, F. Girgsdies, N. Wang, S.B. Hamid, R. Schlogl, D.S. Su, Facile synthesis of carbon nanotube/natural bentonite composites as a stable catalyst for styrene synthesis, Chem. Commun., (2008) 6528-6530.

[48] C.O. Mgbemena, N.O. Ibekwe, A.A.P. Mohamed, R. Sukumar, A.R.R. Menon, Thermal Behavior and UV Properties of Organomodified Kaolin Oleochemically Derived

from Rubber Seed Oils (Hevea brasiliensis) and Tea Seed Oils (Camellia sinensis), Journal of Surface Engineered Materials and Advanced Technology, 03 (2013) 163-168.
[49] R.M. Mohamed, E.S. Baeissa, Mordenite encapsulated with Pt–TiO_2: Characterization and applications for photocatalytic degradation of direct blue dye, J. Alloys Compd., 558 (2013) 68-72.
[50] Y.-H. Hsien, C.-F. Chang, Y.-H. Chen, S. Cheng, Photodegradation of aromatic pollutants in water over TiO_2 supported on molecular sieves, Appl. Catal. B, 31 (2001) 241-249.
[51] T. Noguchi, A. Fujishima, K. Hashimoto, P. Sawunyama, Photocatalytic degradation of gaseous formaldehyde using TiO_2 film, Environ. Sci. Technol., 32:23 (1998) 3831-3833.
[52] X. Gao, I.E. Wachs, Titania–silica as catalysts: molecular structural characteristics and physico-chemical properties, Catal. Today, 51 (1999) 233-254.
[53] D. Chen, Z. Qu, Y. Sun, K. Gao, Y. Wang, Identification of reaction intermediates and mechanism responsible for highly active HCHO oxidation on Ag/MCM-41 catalysts, Appl. Catal., B, 142–143 (2013) 838-848.
[54] G. Busca, J. Lamotte, J.C. Lavalley, V. Lorenzelli, FT-IR study of the adsorption and transformation of formaldehyde on oxide surfaces, J. Am. Chem. Soc., 109 (1987) 5197-5202.
[55] F.J. Gil-Llambias, A.M. Escudey-Castro, Use of zero point charge measurements in determining the apparent surface coverage of molybdena in MoO_3/γ-Al_2O_3 catalysts, J. Chem. Soc., Chem. Commun., (1982) 478-479.
[56] C. Knapp, F.J. Gil-Llambias, M. Gulppi-Cabra, P. Avila, J. Blanco, Phase distribution in titania-sepiolite catalyst supports prepared by different methods, J. Mater. Chem., 7 (1997) 1641-1645.
[57] M.Y. Ahn, T.R. Filley, C.T. Jafvert, L. Nies, I. Hua, J. Bezares-Cruz, Photodegradation of decabromodiphenyl ether adsorbed onto clay minerals, metal oxides, and sediment, Environ. Sci. Technol., 40 (2006) 215-220.
[58] D. Kibanova, M. Trejo, H. Destaillats, J. Cervini-Silva, Photocatalytic activity of kaolinite, Catal. Commun., 12 (2011) 698-702.
[59] J. Yang, D. Li, Z. Zhang, Q. Li, H. Wang, A study of the photocatalytic oxidation of formaldehyde on $Pt/Fe_2O_3/TiO_2$, J. Photochem. Photobiol. A, 137 (2000) 197-202.
[60] H. Liu, Z. Lian, X. Ye, W. Shangguan, Kinetic analysis of photocatalytic oxidation of gas-phase formaldehyde over titanium dioxide, Chemosphere, 60 (2005) 630-635.

[61] Z. Ding, H.Y. Zhu, G.Q. Lu, P.F. Greenfield, Photocatalytic Properties of Titania Pillared Clays by Different Drying Methods, J. Colloid Interface Sci., 209 (1999) 193-199.

[62] N. Takeda, M. Ohtani, T. Torimoto, S. Kuwabata, H. Yoneyama, Evaluation of diffusibility of adsorbed propionaldehyde on titanium dioxide-loaded adsorbent photocatalyst films from its photodecomposition rate, J. Phys. Chem. B, 101 (1997) 2644-2649.

SUPPLEMENTARY INFORMATION

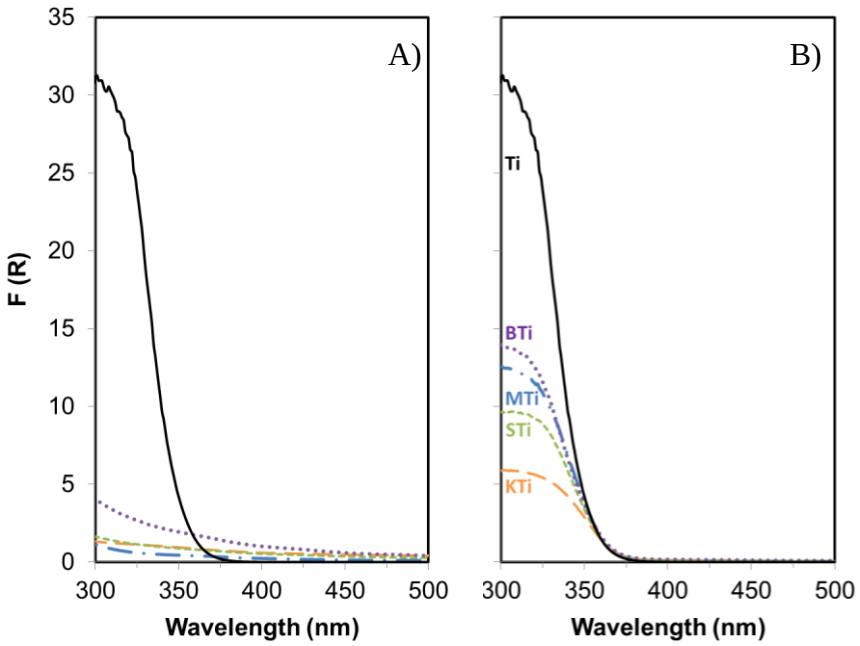

Figure S1. UV-Vis spectra obtained for A) the natural silicates, and B) their composites with TiO_2 treated at 500 ºC: bentonite (····), mordenite (— ·), sepiolite (- - -), and kaolinite (— —).The spectrum of the commercial TiO_2 employed in the composites is added in continuous black line as reference.

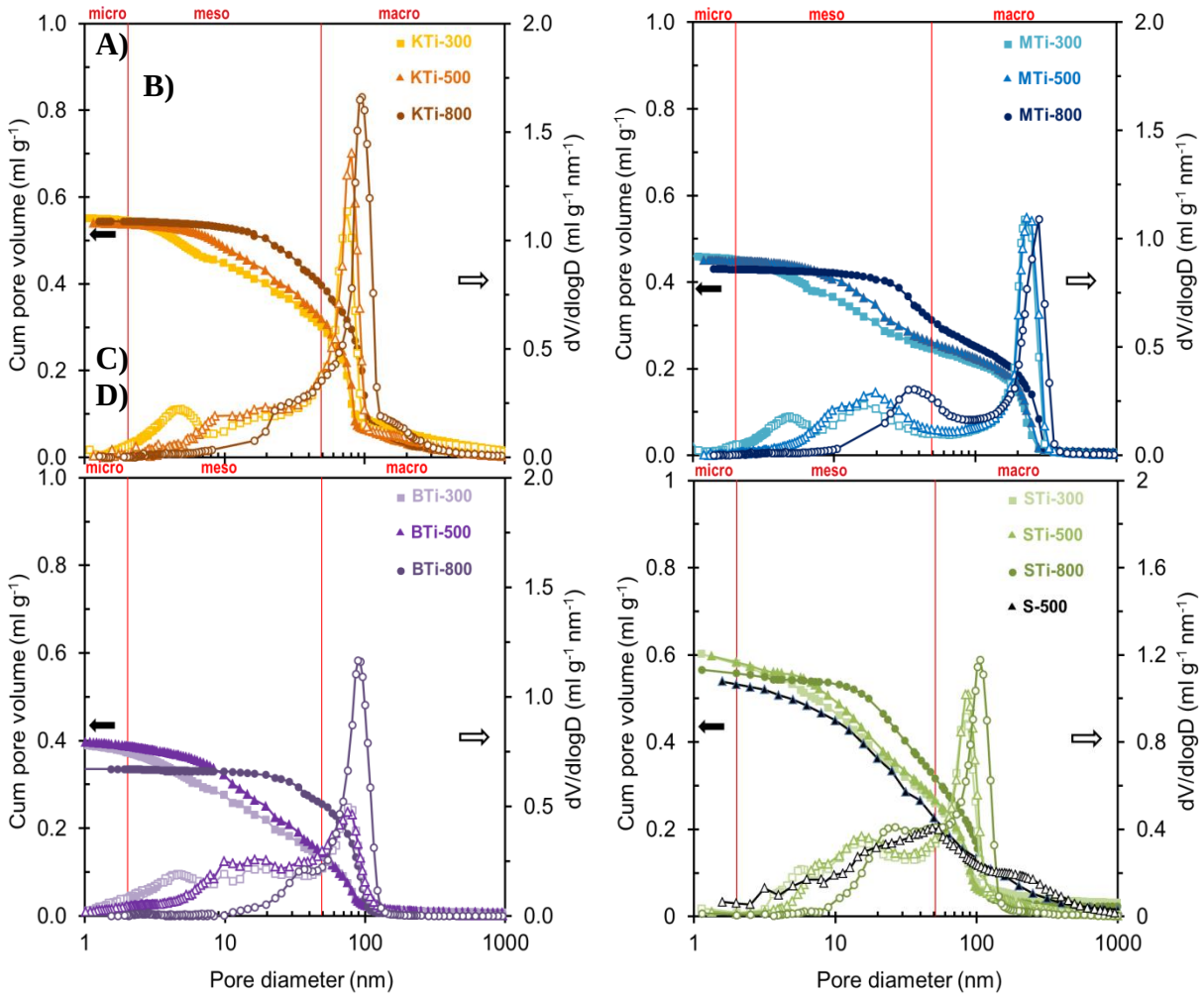

Figure S2. Cumulated pore volume (filled symbols) and pore size distribution (empty symbols) as obtained by combination of N_2 adsorption isotherms and MIP of the silicate-TiO_2 hybrids treated at different temperatures for: A) kaolinite, B) mordenite, C) bentonite, D) sepiolite. In the latter, the curves of pure sepiolite extrudates treated at 500 ºC are included for comparison.

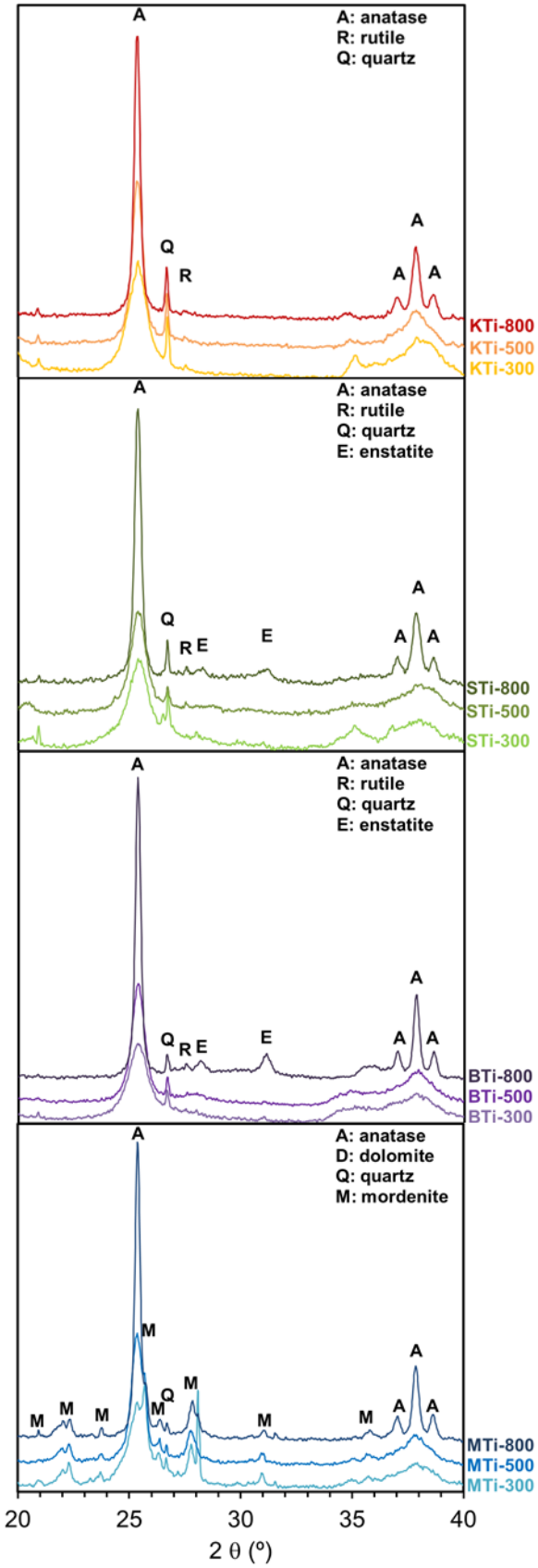

Figure S3. XRD pattern of the TiO_2-silicate composites treated at different temperatures.

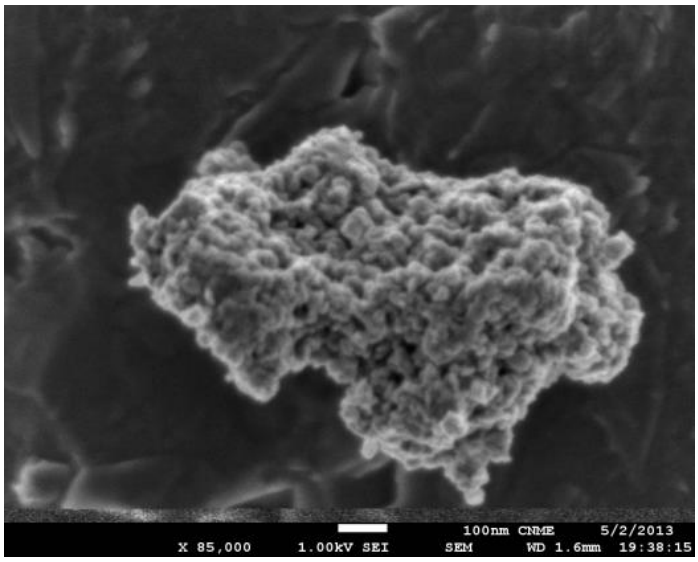

Figure S4. Micrograph of commercial TiO_2 aggregate obtained by SEM microscopy.